Arxiv: 2301.11060

Bubbles and outflows: the novel JWST/NIRSpec view of the z=1.59 obscured quasar XID2028

G. Cresci[1], G. Tozzi[2,1], M. Perna[3], M. Brusa[4,5], C. Marconcini[2,1], A. Marconi[2,1], S. Carniani[6], M. Brienza[5,4], M. Giroletti[7], F. Belfiore[1], M. Ginolfi[2,1], F. Mannucci[1], L. Ulivi[2,1], J. Scholtz[8,9], G. Venturi[10,1], S. Arribas[3], H. Übler[8,9], F. D'Eugenio[8,9], M. Mingozzi[11], B. Balmaverde[12], A. Capetti[12], E. Parlanti[6], and T. Zana[6]

ABSTRACT

Quasar feedback in the form of powerful outflows is invoked as a key mechanism to quench star formation in galaxies, although direct observational evidence is still scarce and debated. Here we present Early Release Science JWST NIRSpec IFU observations of the z=1.59 prototypical obscured quasar XID2028: this target represents a unique test case to study QSO feedback at the peak epoch of AGN-galaxy co-evolution thanks to its existing extensive multi-wavelength coverage and massive and extended outflow detected both in the ionised and molecular components. With the unprecedented sensitivity and spatial resolution of JWST, the NIRSpec dataset reveals a wealth of structures in the ionised gas kinematics and morphology previously hidden in the seeing-limited ground-based data. In particular, we find evidence of interaction between the interstellar medium of the galaxy and the QSO-driven outflow and radio jet, which is producing an expanding bubble from which the fast and extended wind detected in previous observations is emerging. The new observations confirm the complex interplay between the AGN jet/wind and the ISM of the host galaxy, highlighting the role of low luminosity radio jets in AGN feedback, and showcase the new window opened by NIRSpec on the detailed study of feedback at high redshift.

Background:

1. Massive and fast outflows are almost ubiquitous in luminous galaxies (ultrafast X-ray outflows; atomic, molecular and ionized gas outflows).

These outflows may suppress SF activity (removing and heating ISM).

[Not direct observation on how outflows affects SF.]

2. SF activities are peak at z~2 → AGN feedback is expected to reach its maximum efficiency.

AGN-driven outflows depends on ISM properties and gas content.

[z~2: Difficult to be observed from ground-based telescope.]

Target:

XID2028 (z=1.5930): one of the best-studied objects in feedback phase

Type 1.8-1.9 quasar, Broad Line Region (BLR) are strongly obscured

M_*~$4.5\times10^{11} M_\odot$, SFR~$250 M_\odot/yr$

SINFONI-IFU: A massive ($\dot{M}_{out,ion}$~$300 M_\odot/yr$) and extended (~13 kpc) ionized outflow, traced by [OIII]5007 emission.

ALMA (*Brusa+18*): M_{gas}~$10^{10} M_\odot$, a galaxy-scale molecular outflow

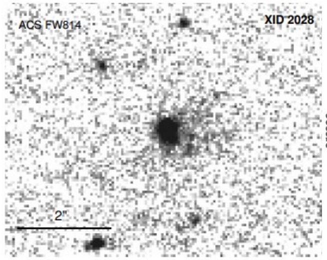

HST/ACS in Brusa+10

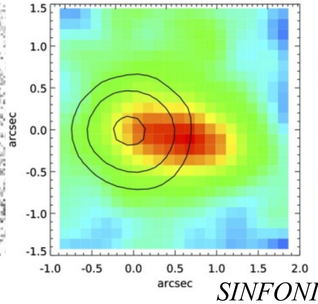

SINFONI-IFU in Cresci+15

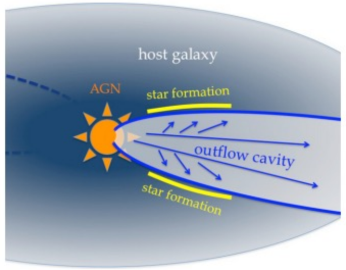

JWST observation: The Q-3D ERS Proposal

The NIRSpec IFU: Obs Time ~2.95 hrs, 0.97-1.82μm at R~2700, 3"×3" FOV with 0.1"×0.1" spatial elements

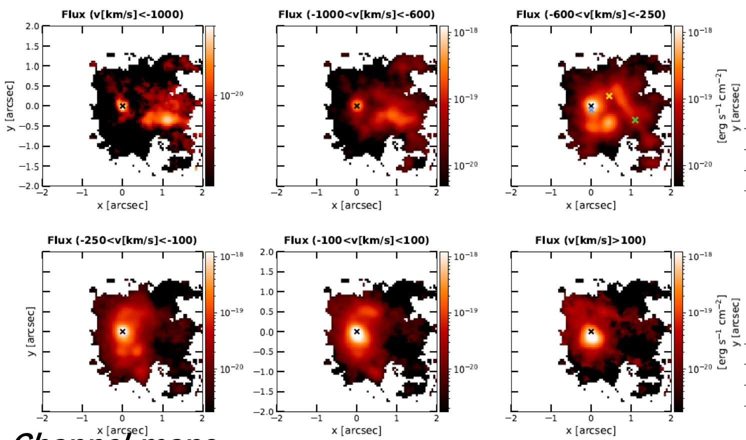

Channel maps

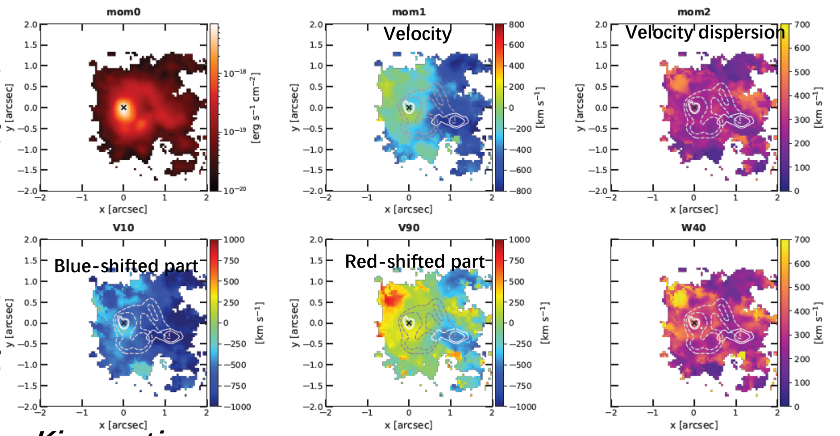

Kinematics maps W40 = v50 -v10, line width containing 40% of the emission line

Result:

1.Bubbles and outflows: extended ionized gas kinematics

A prominent, collimated blue emission is evident in the most blue-shifted velocity bin. (Also seen in Cresci+15)

At lower blue-shifted (-600, -250), a cavity of suppressed line emission becomes evident between QSO and outflow, which also form a filaments-like structure.

From v90 map, gas is outflowing in opposite directions from the central source at Northwest.

Highly blue-shifted emission at Northwest + a possible continuum source → A possible companion galaxy (not likely)

3. ISM properties ([SII]6716,30 line ratio, Hα/Hβ, BPT)

The electron density seems uniform (S/N > 3).

The outflow region: n_e~$360 \pm 180 cm^{-3}$.

The extinction seems to decrease towards the nucleus. The extinction is also decreasing along the filaments, where shocks might contribute to destroying the dust. The outflow region: $A_V = 1.1 \pm 0.5$

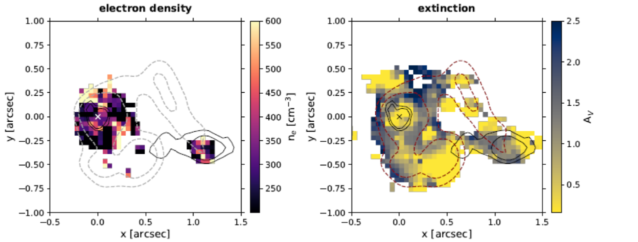

6. Outflow energetics and mass outflow rate

Ionized outflow (n_e from [SII], Hα based measurement)

$$M_{out} = 3.2 \cdot 10^5 \left(\frac{L_{out}(H\alpha)}{10^{40}\ erg/s}\right)\left(\frac{100\ cm^{-3}}{n_{e,out}}\right) M_\odot, \quad \dot{M}_{out,ion} = v_{out}\frac{M_{out}}{R_{out}} = 6 \pm 3\ M_\odot/yr.$$

Difference from Cresci+15, n_e estimation

→ a large difference on M_{out}

For each spaxel, exclude the Gaussian components with |v|<300 km/s and σ < 300 km/s

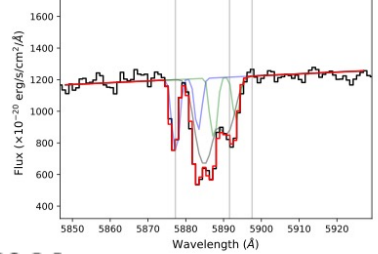

Neutral outflow (NaID5890,5896)

Three distinct blue-shifted components in absorption

$$\dot{M}_{out,neut} = 7 \cdot \sum_{i=1}^{3}\left(\frac{N_{H,i}}{10^{20}\ cm^{-2}}\right)\left(\frac{R}{5\ kpc}\right)\left(\frac{v_{0,i}}{300\ km/s}\right) \sim 30\ M_\odot/yr,$$

Molecular outflow (Brusa+18)

$\dot{M}_{out,mol} \sim 20 - 120\ M_\odot/yr$

→ $\dot{M}_{out,tot} \sim 60 - 160\ M_\odot/yr.$

$\tau_{depl} = M_{gas}/(SFR + \dot{M}_{out,tot}) \sim 30$ Myr.

5. Modeling the observed gas kinematics with MOKA3D

To test if the shell and piercing jet geometry predicted by simulations can be applied to XID2028, comparing the NIRSpec XID2028 data to the 3D AGN outflow model generated using MOKA3D (Modelling Outflows Kinematics in AGN 3D).
How the observed gas geometry can be reproduced using an expanding bubble dragged by the jet and the wind, plus a collimated outflow where the radio jet escapes the host galaxy ISM.
The estimate of the intrinsic, deprojected outflow velocity in the best fitting model is 1027 km/s, with an aperture angle α = 10°
The bubble and outflow system is reproduced with an inclination of ∼ 27° with respect to the observer's line of sight.

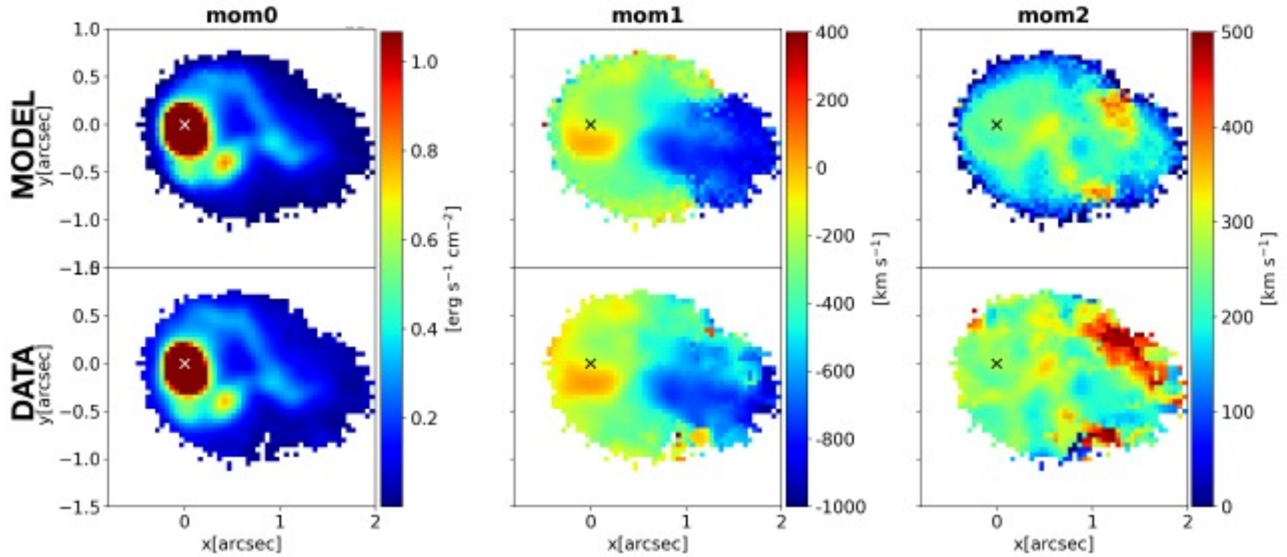

6. Outflow energetics and mass outflow rate

Ionized outflow (n_e from [SII], Hα based measurement)

$$M_{out} = 3.2 \cdot 10^5 \left(\frac{L_{out}(H\alpha)}{10^{40}\ \mathrm{erg/s}}\right)\left(\frac{100\ \mathrm{cm}^{-3}}{n_{e,out}}\right) M_\odot, \quad \dot{M}_{\mathrm{out,ion}} = v_{\mathrm{out}} \frac{M_{\mathrm{out}}}{R_{\mathrm{out}}} = 6 \pm 3\ M_\odot/\mathrm{yr}.$$

Close to the estimation from MOKA3D

Excluding in each spaxel the Gaussian components with a velocity shift |v|<300 km/s and σ < 300 km/s
Difference from Cresci+15, n_e estimation → a large difference on M_{out}

2. A possible rotating disk in the host galaxy: Consistent with the molecular gas by B18 in CO(5-4)

Neutral outflow (NaID5890,5896)
Three distinct blue-shifted kinematic components in absorption

$$\dot{M}_{\mathrm{out,neut}} = 7 \cdot \sum_{i=1}^{3}\left(\frac{N_{H,i}}{10^{20}\ \mathrm{cm}^{-2}}\right)\left(\frac{R}{5\ \mathrm{kpc}}\right)\left(\frac{v_{0,i}}{300\ \mathrm{km/s}}\right) \sim 30\ M_\odot/\mathrm{yr},$$

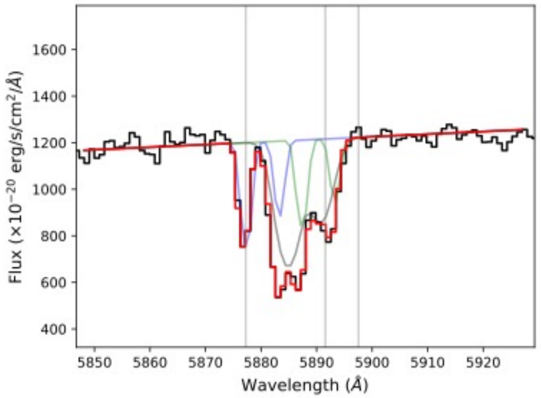

Molecular outflow:
Brusa+18: $\dot{M}_{\mathrm{out,mol}} \sim 20 - 120\ M_\odot/\mathrm{yr}$

$$\dot{M}_{\mathrm{out,tot}} \sim 60 - 160\ M_\odot/\mathrm{yr}.$$

Suppose SFR = 250 $M_\odot/yr$

$$\tau_{\mathrm{depl}} = M_{\mathrm{gas}}/(\mathrm{SFR} + \dot{M}_{\mathrm{out,tot}}) \sim 30\ \mathrm{Myr}.$$

is remarkably smaller than typical gas depletion times in normal star-forming galaxies

4. Jet-ISM interaction in XID2028

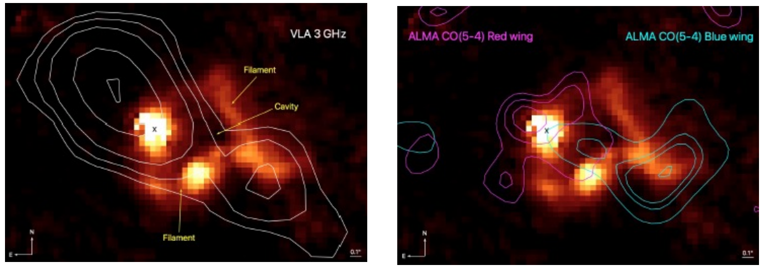

VLA 3 GHz observations show two extended radio lobes broadly coincident with the bi-polar outflows, suggesting the presence of low-luminosity radio jets in the galaxy. The filamentary structure is a hot, expanding bubble filled with low surface brightness emission brightened at the edges, which is inflated and dragged by the jet into the galaxy ISM.
At a larger radius, the jet appears to have pierced the shell, and it propagates faster through the lower-density environment;

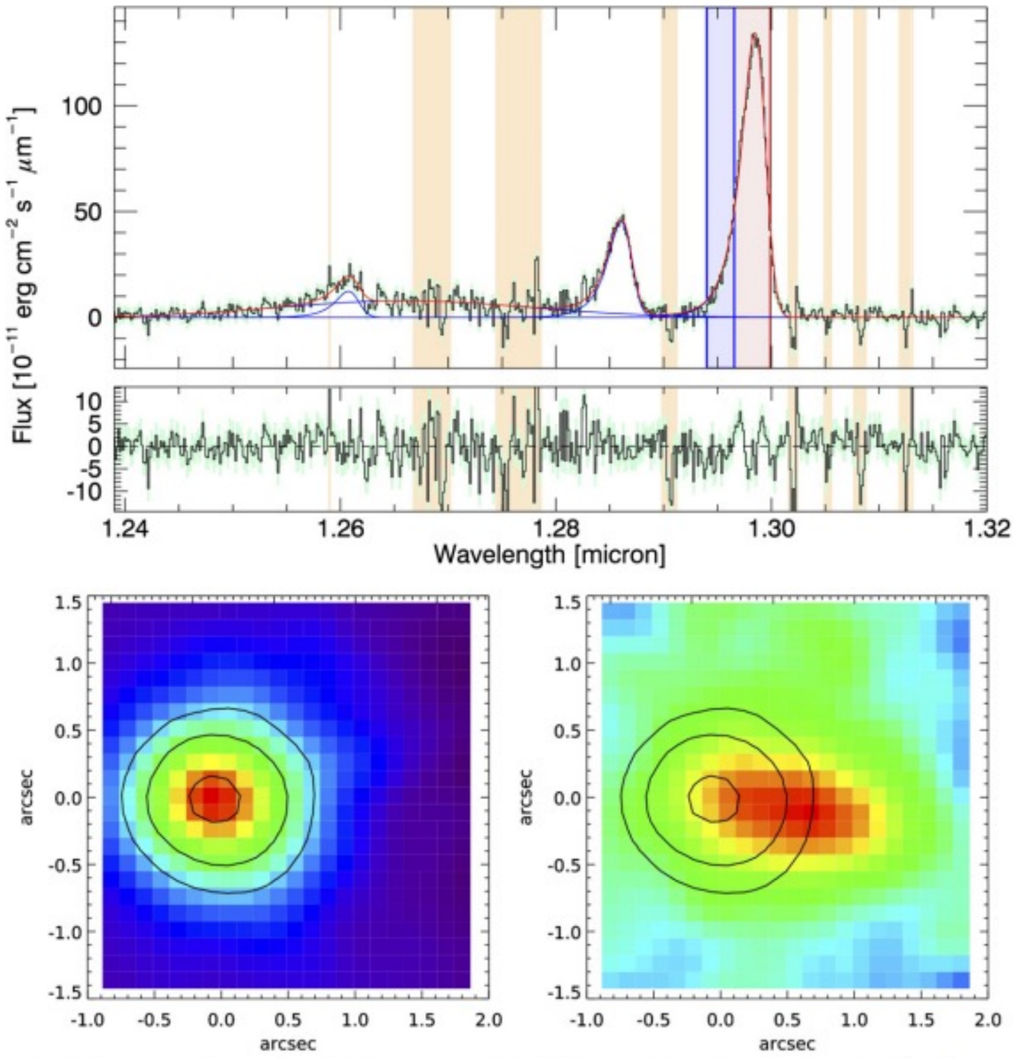

Figure 1. [O III] in XID2028. Upper panels: the *J*-band SINFONI spectrum of XID2028, integrated in a region of 8 × 8 spaxels (1″ × 1″) around the QSO. The observed spectrum is shown in black, the different broken power-law components in the fit for each line (Hβ, large BLR Hβ, [O III] $\lambda\lambda$4959, 5007) are shown in blue, while their sum is shown in red. The shaded regions show the location of sky lines, that were excluded from the fit. The red and blue box show the intervals in wavelength in which the maps shown in the lower panels are integrated. The residuals of the fit, i.e., the difference between the observed and the model spectrum, are shown below. Lower panels: [O III] λ5007 channel maps obtained integrating the continuum subtracted SINFONI data cube on the line core ($1.296 < \lambda < 1.300$ μm, left, see red box) and on the blue wing ($1.294 < \lambda < 1.296$ μm, right, see blue box). The contours on the line core (levels 0.3, 0.5, 0.9 relative to the peak), marking the position of the central QSO, are shown in black in both panels. The fully resolved, extended blue wing due to the outflow is extended up to 1.″5, i.e., 13 projected kiloparsecs from the QSO position. North is up and east is left, 1″ corresponds to 8.5 kpc.

Cresci+15, SINFONI IFU observations

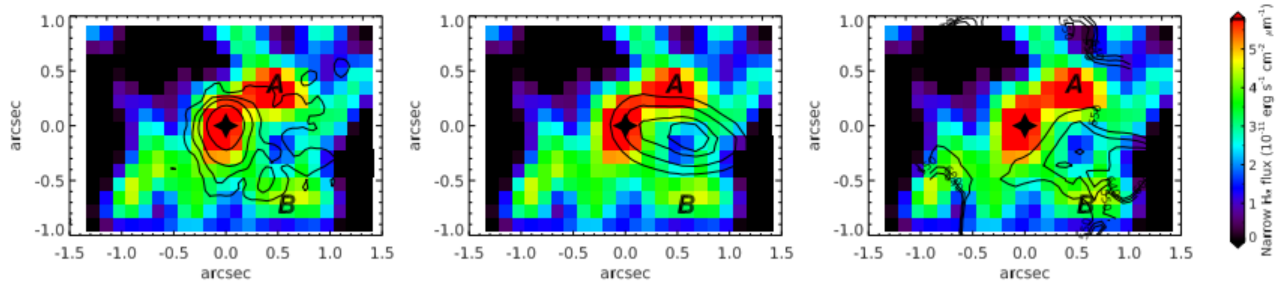

Figure 4. Narrow Hα map. The map is obtained integrating the single broad Gaussian Hα fit residuals on the spectral channels $1.7015 < \lambda < 1.7047$ μm. In the left panel the *HST*/ACS rest frame *U* band contours are superimposed in black (ACS level relative to the peak are 0.008, 0.015, 0.022, 0.05, 0.1, 0.5). The same pattern is obtained by these two independent tracers of star formation in the host galaxy, with two additional clumps of star formation (marked with A and B) elongated at the west of the QSO (marked with a star). In the central panel the blue wing contours from Figure 1, tracing the outflow position, are plotted for comparison. A clear anti-correlation between the outflow location and the star formation tracers suggests that the outflowing material is sweeping the gas along the outflow core ("negative feedback"), while is compressing the gas at its edges inducing star formation at the locations marked as *A* and *B* on the map ("positive feedback"). The right panel shows the W_{40} lie width contours (i.e., the velocity width of the line that contains 80% of the emission line flux such that $W_{40} = v_{50} - v_{10}$, where v_{50} and v_{10} are the velocities at the fiftieth and tenth percentiles, respectively; velocity levels 900, 1000, 1200 km s^{-1}) overplotted on the narrow Hα residuals. It can be seen how the shape of the Hα residuals, including the discontinuity between the central clump and the south west one, is anti correlated with regions of large line emission, $W_{40} > 550$ km s^{-1}, due to the outflowing gas.

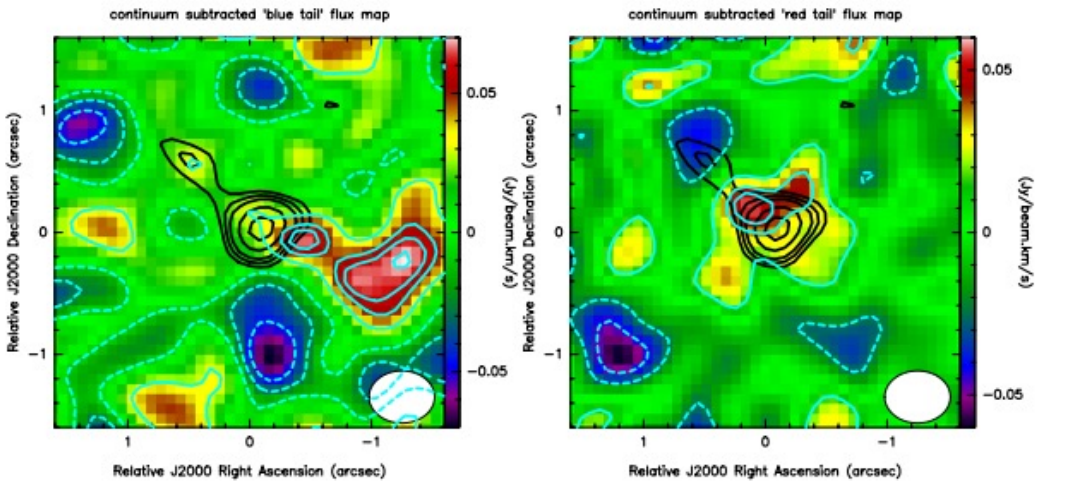

Fig. 9. Flux maps extracted by collapsing the channels in the range [$v < -350$ km s^{-1}] (blue tail; *left panel*), and [$v > 350$ km s^{-1}] (red tail; *right panel*). The images are extracted from the natural flux maps to maximise the sensitivity to detect faint features. The cyan contours represent the sigma levels: −1, −2, −3 (dashed) 1, 2, 2.5, and 3 (solid; $1\sigma \sim 0.02$ Jy km s^{-1}). The black contours at 3, 4, 5, 7, and 9σ indicate the dust continuum emission (from Fig. 1). The beam ellipse is drawn in the lower right corner in *both panels*. The colour wedge gives the flux intensity scale in Jy km s^{-1} beam^{-1}.

CO(5-4) line profile from Brusa+18

Data Analysis:

5×5 spaxel (0.25”×0.25”)

Three BLR Gaussian components

For same region, each Gaussian component of all emission lines to have the same line profile shape

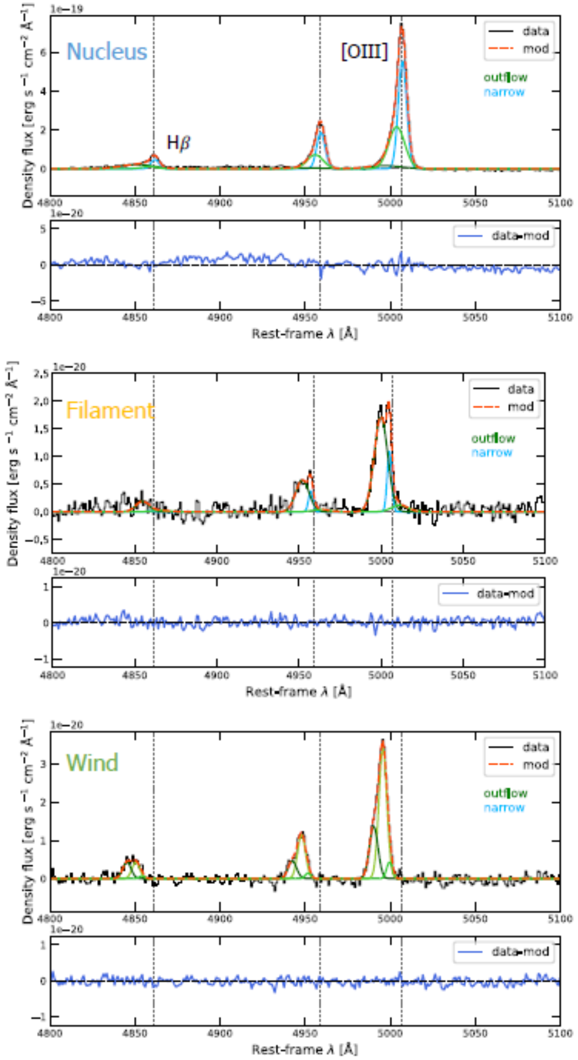

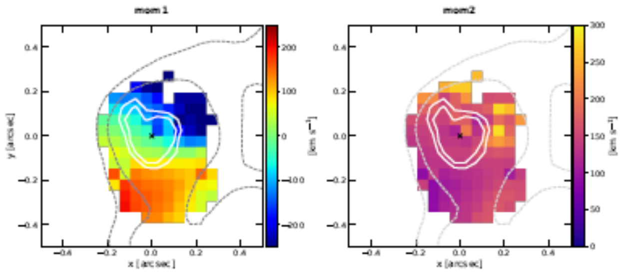

Fig. 5. Moment 1 and Moment 2 maps for the component of the [OIII]λ5007 line emission tracing gas in the host galaxy (see text). The contours are the same as shown in Fig. 4. An S/N>40 threshold has been used to mask lower S/N spaxels and isolate the rotation in the central spaxels. A rotational pattern is suggested by the data, compatible with the CO(5-4) rotation detected by B18.

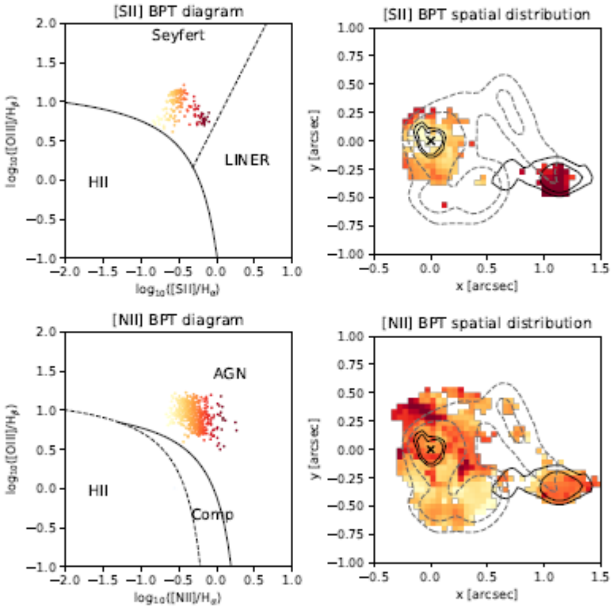

Fig. 7. Resolved S-BPT (upper panels) and N-BPT (lower panel) diagrams for each spaxel with S/N>3 in each line. The data points on the BPT diagrams (left panels) are colour coded as a function of their [SII]/Hα and [NII]/Hα ratios for the S-BPT and N-BPT respectively. The same colours are used in the corresponding maps (right panels), where the contours shown in Fig. 4 are overplotted. The QSO location is marked with a black cross.

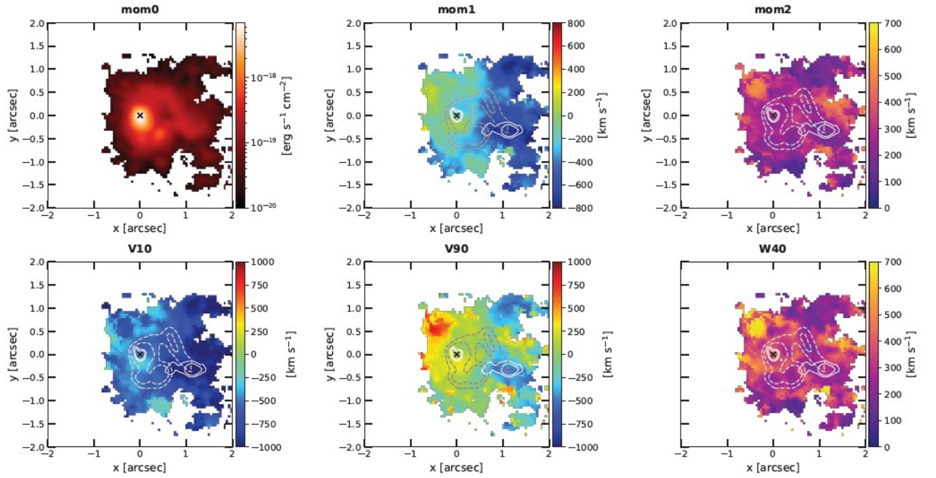

Fig. 4. Kinematics of the [OIII] line emission. The upper panels show Moment 0, Moment 1 and Moment 2 of the whole line profile velocity. The lower panels instead show v_{10}, the velocity at the 10th percentile of the overall emission-line profile in each spaxel, v_{90}, the 90th percentile, and W_{40}, i.e. $W_{40} = v_{50} - v_{10}$, the line width containing 40% of the emission line flux. Solid contours represent the 30% and 50% of the peak emission in the bluest channel map ($v < -1000$ km/s) in Fig. 3, while dashed contours the 5% and 10% emission of the third channel ($-600 < v < -250$ km/s). The maps show the spaxel with S/N>3 on the total [OIII] flux, and the cross marks the position of the QSO.

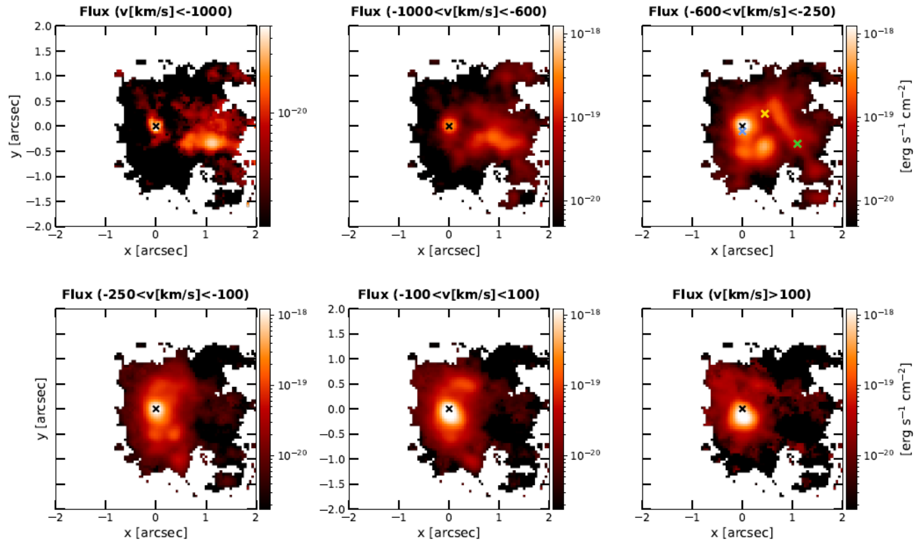

Fig. 3. Channel maps for the [OIII]λ5007 line emission: the six panels show the [OIII] line flux in different velocity bins. In the upper left panel, the highest blue-shifted velocities are shown, highlighting the fastest part of the wind. In the following panels, the filaments connecting the outflow to the quasar location become evident. In contrast, the lower right panel shows the possible red-shifted outflow emission to the northeast. The maps show the spaxel with S/N>3 on the total [OIII] flux. At the distance of the target, the scale is ~ 8.5 kpc/". The coloured crosses show the location of the extraction spaxels for the spectra shown in Fig. 2.